MATERIALS CHEMISTRY FRONTIERS

CHINESE CHEMICAL SOCIETY

ROYAL SOCIETY OF CHEMISTRY

RESEARCH ARTICLE

View Article Online
View Journal | View Issue

Cite this: *Mater. Chem. Front.*, 2025, **9**, 1139

Prolonged irradiation-induced delayed luminescence of PMMA-dispersed imide compounds containing ether- and thioether-bridged cores†

Marina Doi, Haonan Liu and Shinji Ando *

Time variations in the photoluminescence (PL) properties of four types of imide compounds (ICs) with ether (OD-IC), thioether (SD-IC), dibenzofuran (BO-IC), and dibenzothiophene (BS-IC) cores dispersed in polymer films were investigated to elucidate the effects of the introduction of sulfur atoms and the structural rigidity of the ICs on their PL properties under continuous UV irradiation. These ICs exhibit photoactivated delayed phosphorescence (PH) from the excited triplet state (T_1), which is called prolonged irradiation-induced delayed luminescence (PIDL), after a few minutes of induction time, during which only fluorescence is observed. This result is because oxygen quenching efficiency gradually weakens as the ground-state oxygen decreases *via* energy transfer from the ICs in the T_1 state. As compared with the ICs containing ether linkages (OD-IC, BO-IC), the PHs of the ICs containing thioether linkages (SD-IC and BS-IC) were significantly enhanced by the heavy atom effect, and these showed bathochromic (red) shifts of the PL peaks owing to the extended π-conjugation. Furthermore, the ICs containing five-membered cores (BO-IC and BS-IC) demonstrated longer PIDL lifetimes and shorter induction times than those of the ICs containing flexible linkages (OD-IC and SD-IC), owing to their structural rigidity. In particular, BS-IC exhibited an excellent PIDL properties such as the largest intensity (I = 2480), a long lifetime (τ_{PIDL} = 410 ms), and a short induction time (t_{ID} = 1.55 min) owing to the rigid core containing a sulfur atom. Based on the results, this study provides a valuable strategy for developing novel PIDL materials.

Received 4th October 2024,
Accepted 25th January 2025

DOI: 10.1039/d4qm00871e

rsc.li/frontiers-materials

1. Introduction

Phosphorescent (PH) materials have been expected to be applied in bioimaging,[1,2] information security,[3] solar spectrum converters,[4] and optical sensors[5,6] because of their longer emission wavelengths and longer emission lifetimes.[7] However, the excited triplet state (T_1) is easily quenched or deactivated by intermolecular excitation energy transfer, local molecular motion, or excitation energy transfer to surrounding molecules such as triplet oxygen in the atmosphere. Thus, there have been many reports on controlling the photophysical processes associated with the T_1 state to analyse and enhance the PH properties of small molecules. For instance, the heavy atom effect has been widely utilised, in which heavy atoms, such as heavy halogens, chalcogen atoms, and transition and noble metals, are introduced into phosphors to increase the efficiency of intersystem crossing (ISC).[8] When noble metals, such as iridium or platinum, are introduced into luminescent materials, spin–orbit coupling is significantly enhanced, leading to an increased rate constant of ISC (k_{ISC}).[9,10] However, transition or noble metals are expensive and often toxic to the environment and human health. In recent years, metal-free organic molecules exhibiting room-temperature PH (RTP) have been developed by introducing non-metallic heavy atoms into luminescent phosphors to avoid such shortcomings.[4,11–15] We recently reported that introducing heavy halogens, such as bromine or iodine, into the main chain of luminescent polyimides significantly enhances the k_{ISC} and the luminescent intensity of RTP.[4,12,14–16] Chalcogen atoms, including sulfur (S), selenium (Se), and tellurium (Te), are also expected to have strong heavy atom effects due to their sizeable atomic number.[17–20] Gallardo *et al.*[20] reported that the triazine derivatives incorporating thiophene bridges exhibited RTP in solution due to the enhanced ISC by sulfur. Furthermore, Hariharan *et al.*[19] reported that chalcogen-annulated perylene bisimides containing oxygen, sulfur, and selenium increased k_{ISC} with increasing chalcogen atomic numbers (O < S < Se).

Department of Chemical Science and Engineering, Institute of Science Tokyo, Ookayama, 2-12-1-E4-5, Meguro-ku, Tokyo 152-8552, Japan.
E-mail: ando.s.aa@m.titech.ac.jp

† Electronic supplementary information (ESI) available. See DOI: https://doi.org/10.1039/d4qm00871e

Meanwhile, RTP can also be observed by careful suppression of non-radiative (NR) deactivations: The major causes of the NR deactivations are classified as (1) thermal deactivation of triplet excitons by molecular motion,[21–23] (2) intermolecular excitation energy transfer between adjacent polymer chains,[24,25] and (3) excitation energy transfer to the surrounding oxygen (*i.e.*, oxygen quenching, OQ).[21,22,24] Among them, OQ is the energy transfer from the T_1 state of a phosphor to a triplet molecular oxygen ($^3O_2$) in the ground state, followed by excitation of $^3O_2$ to the excited singlet state ($^1O_2$), which is a crucial mechanism to suppress the PH emission in the atmosphere. Ding *et al.*[21] reported that a host–guest system consisting of pyrene derivatives dispersed in a benzophenone (BPO) matrix exhibited long-wavelength RTP (732 nm) owing to the high conjugation of pyrene derivatives, leading to a reduction in the excited triplet energy. The rigid environment in the crystalline BPO and the strong interaction between BPO and the phosphor effectively suppressed the molecular motion, resulting in a longer PH lifetime (τ_P = 324 ms). Reineke *et al.*[24] reported that a phosphor dispersed in poly(methyl methacrylate) (PMMA) covered with polyvinyl alcohol (PVA) exhibited PH after prolonged UV irradiation. They concluded that the PH was caused by the reduced rate constant of OQ (k_Q) owing to the consumption of $^3O_2$ *via* the degradation of PMMA, and the oxygen barrier performance of the PVA coating. Furthermore, Zhao *et al.*[22] achieved RTP with a long emission lifetime (1.2 s) and high quantum yield (Φ = 37.5%) by cross-linking of polymer chains with phosphors, which suppresses the molecular motions and prevents the diffusion of quenchers, *i.e.*, oxygen.

Recently, we have revealed that the imide compounds (ICs) having naphthalene, biphenyl, and oxydiphthalic cores dispersed in PMMA exhibited intriguing delayed photoluminescence (PL) phenomena depending on the UV irradiation time, which is termed as "prolonged irradiation-induced delayed luminescence" (PIDL) (Fig. 1).[26] During the first few minutes of irradiation, called the induction time (t_{ID}), ICs exhibited only fluorescence (FL) because OQ quenched PH, and $^3O_2$ was simultaneously excited to $^1O_2$. Subsequently, some $^1O_2$ was consumed *via* oxidative degradation of PMMA, and the remaining $^1O_2$ was gradually deactivated to $^3O_2$ after accumulation in the excited state for a certain lifetime of $^1O_2$, resulting in a gradual decrease in $^3O_2$. After induction time, the PH process dominated over the OQ process, and the ICs started to exhibit delayed PH, that is, PIDL.

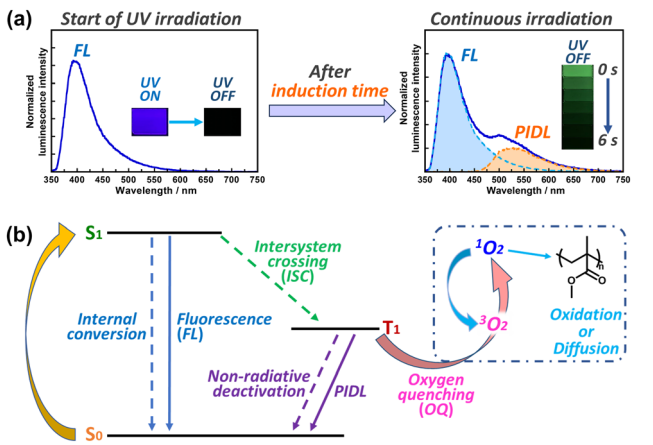

Fig. 1 (a) Variation of emission spectra with continuous UV irradiation and (b) Jablonski diagram based on the photophysical mechanism of PIDL.[26] During the first few minutes of irradiation, ICs exhibit only FL because PH is quenched *via* OQ. After the continuous irradiation, the OQ efficiency decreases, resulting in the emergence of green PIDL.

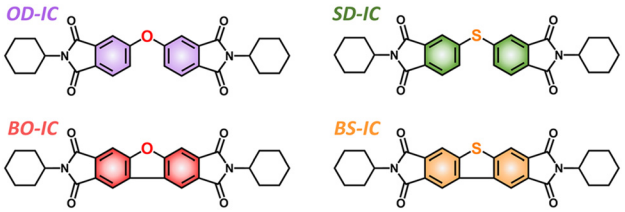

Scheme 1 Chemical structures of ICs.

In this study, we designed and synthesised four types of ICs, *N*,*N*′-dicyclohexyl-4,4′-oxydiphthalic imide (OD-IC), *N*,*N*′-dicyclohexyl-4,4′-thiodiphthalic imide (SD-IC), *N*,*N*′-dicyclohexyldibenzofuran tetracarboxylic diimide (BO-IC), and *N*,*N*′-dicyclohexyldibenzothiophene tetracarboxylic diimide (BS-IC), as shown in Scheme 1. The emission spectra of the PMMA-dispersed films of ICs were measured under continuous UV irradiation, and the rate constant of each photophysical process was evaluated using luminescence lifetime (τ) and quantum yields (Φ) to compare the PIDL properties of the four types of ICs. Based on the photophysical behaviour of the ICs related to their T_1 state, the heavy atom effect caused by the sulfur atoms in their skeletal structures, alongside the differences between the flexible and rigid cores of the ICs were investigated in detail.

2. Experimental

2.1. Materials

4,4′-Oxydiphthalic anhydride (ODPA) provided by MANAC Inc. (Tokyo, Japan) was purified by drying at 150 °C for 5 h *in vacuo*, followed by sublimation under reduced pressure. 4,4′-Thiodiphthalic anhydride (SDPA) provided by Prof. Fang Xingzhong (Ningbo Institute of Materials Technology and Engineering, Chinese Academy of Science, China) was purified by reflux at 100 °C using acetic anhydride. Cyclohexylamine (CHA), hydrochloric acid, potassium hydroxide (KOH), iodine (I_2), potassium iodate (KIO_3), sodium hydrogen carbonate ($NaHCO_3$), potassium fluoride (KF), sodium thiosulfate ($Na_2S_2O_3$), sulfuric acid (H_2SO_4), xylene, ethanol, fuming nitric acid (HNO_3), 40% methylamine solution, *N*,*N*-dimethylformamide (DMF), benzene, propionic acid and ethyl acetate were purchased from Kanto Chemical Co. (Tokyo, Japan); chloroform from Wako Pure Chemical Industries Ltd (Tokyo, Japan); 18-crown-6-ether (18C6) from Tokyo Chemical Industry (TCI) Co. Ltd (Tokyo, Japan); and poly(methyl methacrylate) (PMMA, Sumipex LG, average M_w 50 000–100 000) from Sumitomo Chemical Co. Ltd (Tokyo, Japan). These compounds were used as received without further purification.

2.2. Synthesis of DBOA and DBSA

The detailed synthetic procedures of dibenzofuran tetracarboxylic dianhydride (DBOA) and dibenzothiophene tetracarboxylic dianhydride (DBSA) are described and illustrated in Schemes S1 and S2 in the ESI.†

2.3. Synthesis of imide compounds (ICs)

The synthetic scheme for OD-IC is shown in Scheme S3 (ESI†). CHA (3.3 g, 33.3 mmol) and ODPA (2.9 g, 9.4 mmol) were mixed in propionic acid (50 mL) and stirred for 30 min. The solution was refluxed at 150 °C for 2.5 h under an N_2 flow. After cooling to 22 °C, the solid was filtered, washed with ethanol, and dried under vacuum at 105 °C for 3 h. A white powder of OD-IC was obtained (3.7 g, 7.8 mmol, 83% yield) by recrystallisation from ethyl acetate. The other ICs (SD-IC, BO-IC, and BS-IC in Scheme 1) were prepared similarly by reacting SDPA, DBOA, or DBSA with CHA. White powders of SD-IC (0.4 g, 0.8 mmol, 44% yield), BO-IC (0.1 g, 0.3 mmol, 85% yield), and BS-IC (0.02 g, 0.05 mmol, 68% yield) were obtained. Fig. S1–S8 (ESI†) show the ^{1}H and ^{13}C NMR spectra of the ICs dissolved in DMSO-d_6 and chloroform-*d*.

2.4. Preparation of PMMA-dispersed IC films

PMMA-dispersed films of OD-IC were prepared for the measurement of ultraviolet-visible (UV-vis) absorption, excitation, and emission spectra, emission decay curves, and quantum yield using the following method: PMMA (0.543 g) was dissolved in chloroform (5 mL) by stirring for 3 h. OD-IC (0.00121 g, 0.00256 mmol) was added to the solution and stirred for 24 h. The resulting colourless, transparent solution was spin-coated onto a fused silica substrate with a spinning rate at 200 rpm for 60 s, and then dried at 65 °C for 1 h *in vacuo*. The PMMA-dispersed films of SD-IC, BO-IC, and BS-IC were prepared in the same manner. In these films, the weight fraction of ICs was set to 0.2 wt%.

2.5. Optical measurements

UV-vis absorption and PL excitation/emission spectra were separately measured at 22 °C in air using a JASCO V-760 spectrophotometer (JASCO Co., Tokyo, Japan) and a Hitachi F-7100 FL spectrometer (Hitachi High-Technologies Co., Tokyo, Japan) equipped with an R3896 photomultiplier tube (Hamamatsu Photonics Co., Japan). The front-face method was adopted for the film samples, reducing the self-absorption of the emitted luminescence. The PH spectra were measured in PH mode using a Hitachi F-7100 FL spectrometer. The emission and PH spectra under vacuum were measured using a custom-made vacuum chamber (Akada Industry Co. Ltd, Japan) installed in the FL spectrometer. Spectra were measured after pumping the chamber out using a vacuum pump (Xtradry 150-2, Pfeiffer Vacuum, Germany), and the internal pressure reached approximately 10 Pa after pumping for 30 min.

FL lifetime measurements with a time resolution of <1 ns were conducted using a PL lifetime measurement system (Quantaurus-Tau, C11367-24, Hamamatsu Photonics, Japan) at 22 °C in air. The decay component was recorded upon excitation by applying a flashing light-emitting diode at 340 and 365 nm. FL decay curves were accumulated until the peak intensity reached 1000 counts. The PH lifetimes at 22 °C under vacuum were measured using a xenon flash lamp unit (C11567-02, Hamamatsu, Japan). PH decay curves were recorded under excitation using two bandpass filters (TS OD 4.0-340/25, Edmund Optics Co. Ltd, USA, and FF01-360/12-25, Semrock Inc., USA) with transmission ranges of 334–346 nm and 354–366 nm, respectively. The decay signals accumulated for 5 min. The emission decay curves were fitted using one or two exponential functions so that an indicator for the degree of fitting χ^2 value was in the range of 0.85–1.35. The average lifetime ($\langle\tau\rangle$) was calculated as the intensity-weighted mean lifetime, $\langle\tau\rangle = \sum A_i\tau_i^2/\sum A_i\tau_i$, where A_i is the pre-exponential factor for a lifetime τ_i. The PL quantum yields (Φ) were measured using a calibrated integrating sphere (C9920-02, Hamamatsu Photonics, Japan) connected to a multichannel analyser (C7473-36, Hamamatsu Photonics, Japan) *via* an optical fibre link.

2.6. Optical measurements with continuous irradiation

The PL spectra during and after UV irradiation in air at 22 °C were measured using a home-built optical system, as described in a previous study on PIDL.[26] Spectra were measured at the shutter opening every 100 ms under UV irradiation for 15 min. Fig. S8 (ESI†) shows the detailed measurement method. The PIDL decay curves after continuous UV irradiation were plotted using the intensities of the PIDL in the emission spectra measured every 100 ms after the shutter was closed. The PIDL decay curves were fitted using $I(t) = A \times \exp(t/\tau_{PIDL})$, where $I(t)$ is the PIDL intensity at time t, A is a constant, and τ_{PIDL} is the PIDL lifetime.

The time evolutions of the emission peak areas of FL and PIDL during UV irradiation were estimated by fitting each emission spectrum to a linear combination of the FL and PIDL spectra (Fig. S9, ESI†). The emission spectrum immediately after UV irradiation in air at 22 °C was chosen as the FL spectrum, and the spectrum immediately after the end of UV irradiation for 15 min was chosen as the PIDL spectrum. The induction time, t_{ID}, was estimated as the time from the beginning of UV irradiation to the intersection point of the tangent lines of the change in the area ratio of the PIDL peak during the induction time and the curve at the beginning of the increase in PIDL.

2.7. Nuclear magnetic resonance measurements

Solution-state ^{1}H and ^{13}C NMR spectra were obtained using a JEOL JNMECZ400 spectrometer operating at ^{1}H and ^{13}C resonance frequencies of 400 and 100 MHz, respectively. ^{1}H and ^{13}C chemical shifts (δ_H and δ_C) were calibrated in ppm using tetramethylsilane as the standard (0 ppm).

3. Results and discussion

3.1. Emission of ICs after short UV irradiation

Fig. 2(b) shows the UV-vis absorption spectra of OD-IC, SD-IC, BO-IC, and BS-IC dispersed in PMMA films. The wavelengths of

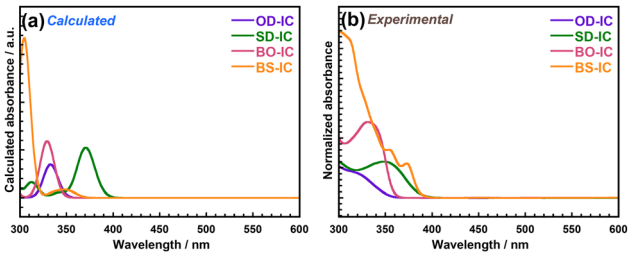

Fig. 2 (a) Calculated and (b) experimental UV-vis absorption spectra for OD-IC, SD-IC, BO-IC, and BS-IC. Experimental absorbances were normalised by the film thickness. IC-dispersed PMMA films were used for the experimental spectra.

the absorption edge (λ_{off}) are summarised in Table 1. The films were colourless and transparent in the visible region because their absorption edges were located in the UV region (<400 nm). This result is attributed to the lower intra- and intermolecular charge transfer interactions suppressed by capping both ends of the dianhydride moiety with two cyclohexyl groups[27,28] and the dispersion in PMMA at a low weight fraction (0.2 wt%). Fig. 2 compares the calculated and experimental UV-vis absorption spectra. Time-dependent DFT (TD-DFT) theory (B3LYP/6-311++G(d,p)) was used for the calculations, and the spectra obtained for OD-IC, SD-IC, and BO-IC reproduced the experimental results well. Conversely, BS-IC showed an absorption peak at 366–406 nm in addition to two absorption peaks at shorter wavelengths (300 and 354 nm), even though it is predicted to show two absorption peaks at 305 and 347 nm and no absorption above 387 nm. This result suggests that the absorption peak at 366–406 nm was attributed to dimers or aggregated molecules in PMMA film owing to the planar structure and strong π–π interactions of BS-IC. Such attribution is supported by the wavelength range of the corresponding absorption band (366–406 nm) very close to that of the excitation spectrum of BS-IC in the solid powder state (390 nm) (Fig. S10, ESI†). The λ_{off} of thioether-bridged SD-IC and BS-IC (413, 406 nm) in PMMA were red-shifted by the incorporation of sulfur atoms compared to the ether-bridged OD-IC and BO-IC (369, 372 nm) (Table 1). This occurrence originates from the extended π-conjugation by the lone pair electrons of the sulfur atom, which lowers the transition energy from the ground state (S_0) to the excited singlet state (S_1).[29] This is supported by the fact that the calculated transition energies ($\Delta\varepsilon$) from the highest occupied molecular orbital (HOMO; ε_{HOMO}) to the lowest unoccupied molecular orbital (LUMO; ε_{LUMO}) for SD-IC and BS-IC (3.93, 4.09 eV) are smaller than those of OD-IC and BO-IC (4.35, 4.32 eV) (Fig. 3).

Fig. 4 shows the excitation/emission spectra of the ICs dispersed in PMMA, measured at 22 °C in air. All ICs exhibited blue emission at 385–415 nm upon excitation with UV light. Table 1 summarises the values of peak wavelengths of the excitation and emission (λ_{ex}, λ_{em}) and Stokes shifts (ν) obtained from the spectra in Fig. 4 and PL quantum yields (Φ). The decay curve of the luminescence intensity at each peak was measured and fitted to one or two exponential components to determine these blue emissions and estimate the average lifetime.

Table 1 Absorption edges, excitation and emission wavelengths (λ_{off}, λ_{ex}, λ_{em}), Stokes shifts (ν), quantum yields (Φ), fluorescence lifetime (τ_F) in air, and phosphorescence lifetime (τ_P) under vacuum for OD-IC, SD-IC, BO-IC, and BS-IC dispersed in PMMA films

Sample	λ_{off} [nm]	λ_{ex} [nm]	λ_{em} [nm]	ν [cm^{-1}]	Φ	τ_F [ns]	τ_P [ms]
OD-IC	369	330	390	4662	0.09[a]	5.92[d,h]	227[f,h]
			480	9470			
SD-IC	413	360	415	3681	0.08[b]	1.04[e,h]	48[g,h]
			500	7778			
BO-IC	372	350	385	2597	0.11[b]	1.48[d,h]	362[f,h]
			470	7295			
BS-IC	406	375	400	1667	0.05[c]	0.88[e,h]	135[g,h]
			480	5833			

[a] Irradiation wavelength, λ_{ir} = 340 nm. [b] λ_{ir} = 360 nm. [c] λ_{ir} = 380 nm. [d] FL lifetime (λ_{ir} = 340 nm) observed at λ_{em}. [e] FL lifetime (λ_{ir} = 365 nm) observed at λ_{em}. [f] PH lifetime (λ_{ir} = 340 nm) observed at λ_{em} under vacuum. [g] PH lifetime (λ_{ir} = 360 nm) observed at λ_{em} under vacuum. [h] Average lifetime estimated from the emission decay curves.

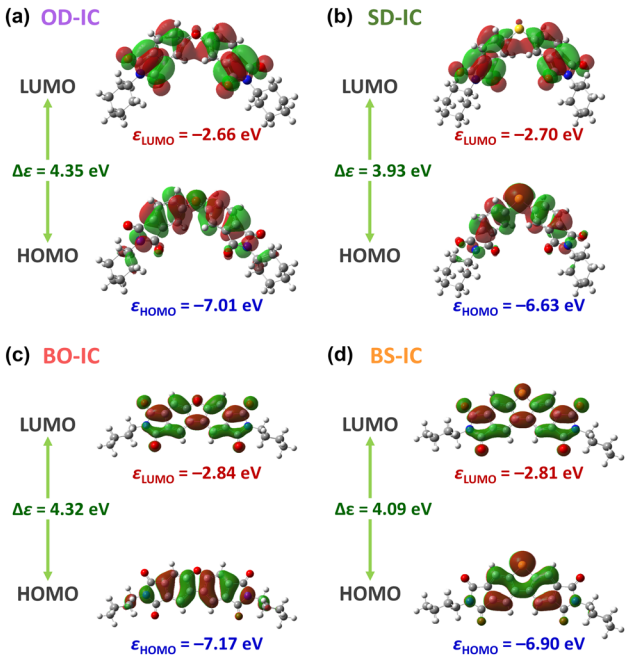

Fig. 3 Spatial distributions of molecular orbitals (MO) calculated using the TD-DFT theory (B3LYP/6-311++G(d,p)) for (a) OD-IC, (b) SD-IC, (c) BO-IC, and (d) BS-IC. ε_{HOMO}, ε_{LUMO}, and $\Delta\varepsilon$ denote the calculated MO energies of LUMO and HOMO and the energy gaps, respectively.

The experimental section describes the fitting procedure. Tables S1 and S2 (ESI†) list the fitted parameters, while Table 1 reports the average lifetime (τ). The bright blue luminescence of these ICs in air is readily attributable to the FL emitted from the S_1 states because their relaxation lifetimes are in the order of nanoseconds (0.88–5.92 ns). In contrast, ICs under vacuum exhibited green broad emission at 470–500 nm in addition to FL, which is attributed to PH due to their significantly long lifetimes (τ_P = 48–362 ms), as shown in Fig. 5. The appearance of PH was induced by the absence of OQ owing to the removal of oxygen under vacuum.

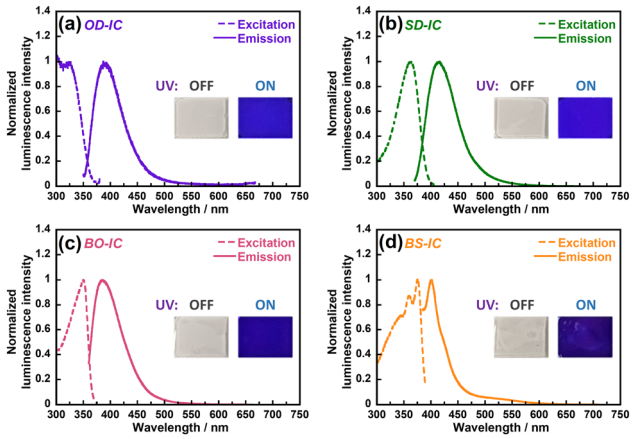

Fig. 4 Excitation/emission spectra for (a) OD-IC, (b) SD-IC, (c) BO-IC, and (d) BS-IC dispersed in PMMA films in air. The excitation wavelength (λ_{ex}) for the emission spectra and the monitoring emission wavelength (λ_{em}) for the excitation spectra are summarised in Table 1. Insets are photos of the films under irradiation of white light (UV OFF) and UV light (λ = 365 nm) (UV ON).

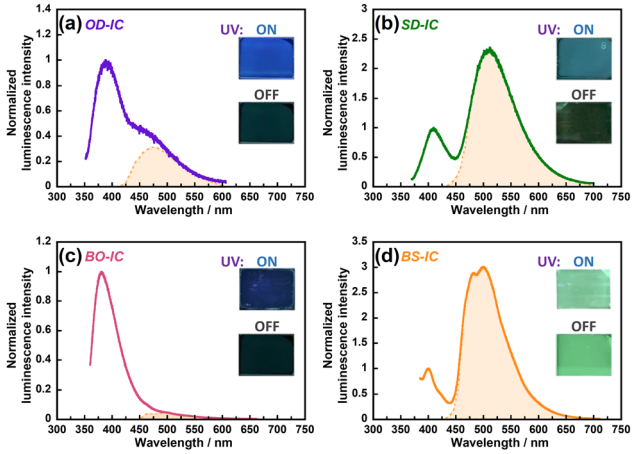

Fig. 5 Emission spectra for (a) OD-IC, (b) SD-IC, (c) BO-IC, and (d) BS-IC dispersed in PMMA films under vacuum. The λ_{ex}s are summarised in Table 1. The areas hatched in orange indicate PH spectral components. Insets are photos of the films under vacuum (UV ON) and just after ceasing UV irradiation (UV OFF).

The optical properties of thioether-bridged SD-IC and BS-IC were compared with those of ether-bridged OD-IC and BO-IC to investigate the effect of incorporating sulfur atoms into the IC skeleton. The λ_{ex} and λ_{em} of FL of the former (λ_{ex} = 360, 375 nm, λ_{em} = 415, 400 nm) were observed at longer wavelengths than those of the latter (λ_{ex} = 330, 350 nm, λ_{em} = 390, 385 nm) (Table 1). This result is due to the decrease in transition energies, $\Delta\varepsilon$, in agreement with the order of λ_{off}.[29] Furthermore, the former ICs showed stronger intensities with shorter emission lifetimes of PH than the latter ICs. This trend can be attributed to the sulfur atoms promoting ISC and the subsequent deactivation process from the T_1 state to the S_0 state.[17,19,30] After all, both are spin-forbidden processes between the singlet and triplet states.

Furthermore, OD-IC and SD-IC have bent and flexible structures owing to their ether and thioether linkages, facilitating local structural relaxation in the excited states accompanied by conformational changes.[31,32] As a result, the S_1 and T_1 energies of these ICs are lowered, leading to an increase in the Stokes shift of FL (ν_f) and PH (ν_p), as shown in Table 1 (OD-IC: ν_f = 4662 cm^{-1}, ν_p = 9470 cm^{-1}, SD-IC: ν_f = 3681 cm^{-1}, ν_p = 7778 cm^{-1}). In contrast, BO-IC and BS-IC have rigid five-membered rings at the centre of their molecules, which strongly restrict their internal rotational and fluctuating motions. Therefore, the Stokes shifts of FL and PH for BO-IC and BS-IC become relatively small (BO-IC: ν_f = 2597 cm^{-1}, ν_p = 7295 cm^{-1}, BS-IC: ν_f = 1667 cm^{-1}, ν_p = 5833 cm^{-1}). Notably, BO-IC only exhibited a weak PH under vacuum, as shown in Fig. 5, suggesting that its OQ efficiency was low, and the effect of suppressing NR deactivation was limited. In contrast, BS-IC showed a significant increase in PH under vacuum, indicating that OQ was efficient and that NR (= OQ) deactivation was inhibited effectively under vacuum. In addition, the rigid structure of BS-IC may result in an intense PH owing to the suppression of molecular motion and the associated low efficiency of NR deactivation. Such differences in the PH properties are discussed in detail in Section 3.2, based on the estimated rate constants relating to the T_1 state.

3.2. Emission of ICs after continuous UV irradiation

Table 2 summarises the rate constants of each photophysical process (k_x) related to the T_1 state in Scheme 2: k_{ISC} for the ISC process, k_P for the PH process, k_{TS} for the NR deactivation from the T_1 state except for OQ, k_Q for OQ in the T_1 state.[7,26] Each rate constant was estimated from the measurements of luminescence quantum yield and lifetime. ESI† describes the detailed calculation procedures. Here, k_Q, the product of k_q and $[^3O_2]$, is listed in Table 2 because only $k_q{\cdot}[^3O_2]$ can be estimated from the analytical and optical measurements under controlled atmosphere conditions, where k_q is the rate constant of energy transfer from the IC in the T_1 state to $^3O_2$ in the ground state, and $[^3O_2]$ is the concentration of $^3O_2$ around ICs in PMMA film. Furthermore, the NR deactivation from the T_1 state can fall under three types: OQ, thermal deactivation owing to molecular motion, and energy transfer between the phosphors. k_{TS} represents only the rate constant related to the molecular motion. This result is because k_{TS} was estimated under vacuum conditions with suppressed OQ, and IC was monodispersed at low concentrations in the PMMA film, suppressing energy transfer between the ICs.

Fig. 6 shows the time evolution of the emission spectra of the PMMA-dispersed OD-IC, SD-IC, BO-IC, and BS-IC during continuous UV irradiation for 15 min in air. The irradiation wavelengths (λ_{ir}s) were set to 340 nm for OD-IC and BO-IC and

Table 2 Rate constants (k_x) for OD-IC, SD-IC, BO-IC, and BS-IC dispersed in PMMA films in air

Sample	k_{ISC} [s^{-1}]	k_P [s^{-1}]	k_{TS} [s^{-1}]	k_Q [s^{-1}]
OD-IC	6.02 × 10^7	0.910	3.49	83 800
SD-IC	57.1 × 10^7	4.710	16.1	1 04 000
BO-IC	24.8 × 10^7	0.004	2.76	84 700
BS-IC	75.5 × 10^7	0.860	6.55	1660

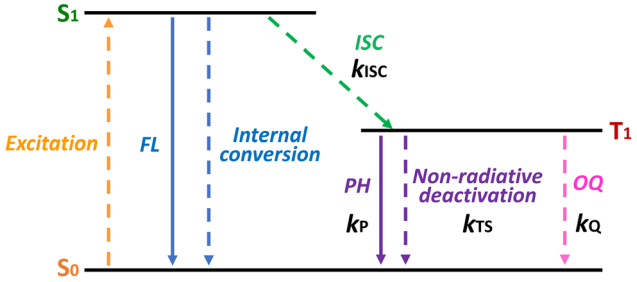

Scheme 2 Jablonski diagram and rate constants of photophysical processes.

365 nm for SD-IC and BS-IC. The optical power density of the light source was set at 2.0 mW cm^{-2}. All ICs exhibited distinguishable PIDL peaks after continuous UV irradiation, and these PIDL peaks were attributed to the PH from the T_1 state, as in previous studies, because the spectral shapes and peak wavelengths of these PIDL were the same as the PH spectra observed under vacuum (Fig. S13, ESI†), similar to our previous study.[26] The thioether-bridged SD-IC and BS-IC showed a more intense PIDL than the ether-bridged OD-IC and BO-IC, which indicated that a large number of triplet excitons were generated in the former owing to the high rate constants of ISC (OD-IC: $k_{ISC} = 6.02 \times 10^{-7}$ s^{-1}, BO-IC: 24.8×10^{-7}, SD-IC: 57.1×10^{-7}, BS-IC: 75.5×10^{-7}), which was enhanced by the heavy atom effect of sulfur.

Fig. 6 shows that BO-IC exhibited much weaker PIDL than OD-IC. This result is contradictory to the fact that the former should produce more triplet excitons because of the smaller k_{TS} of BO-IC associated with molecular motion due to the rigid molecular structure (BO-IC: $k_{TS} = 2.76$ s^{-1}, OD-IC: 3.49 s^{-1}) and the larger k_{ISC} than OD-IC (BO-IC: $k_{ISC} = 24.8 \times 10^{-7}$ s^{-1}, OD-IC: 6.02×10^{-7} s^{-1}). The main reason for this was the difference in the rate constants of deactivation from the T_1 state. Although the rate constants of 'non-radiative' deactivations are similar for both BO-IC and OD-IC (BO-IC: k_{TS} = 2.76 s^{-1}, OD-IC: 3.49 s^{-1}), those of 'radiative' deactivation (PH) for BO-IC is much smaller than that for OD-IC (BO-IC: $k_P = 0.004$ s^{-1}, OD-IC: 0.910 s^{-1}). Therefore, BO-IC is easily deactivated from the T_1 state by NR deactivation, and BO-IC showed a much weaker PIDL after the induction time. ISC process occurs with spin conversion induced by mixing of π- and σ-orbitals,[33,34] and is promoted by structural distortion or conformational change of luminophores. Therefore, the smaller k_P of BO-IC compared with OD-IC is explainable by the suppression of σ–π mixing due to the rigid planar structure. The k_P of BS-IC was smaller than that of SD-IC for the same reason but not as small as that of BO-IC. This trend is due to the PH process enhanced by the heavy atom effect of sulfur. Furthermore, BS-IC showed a more intense PIDL than SD-IC, owing to its smaller k_{TS} and k_Q (rate constant of OQ) values. Because of the smaller k_{TS} (BS-IC: 6.55 s^{-1}, SD-IC: 16.1 s^{-1}), BS-IC is more likely to show PIDL after the extinction of OQ, *i.e.* induction time. In addition, because of the much smaller k_Q of BS-IC (1660 s^{-1}) than that of SD-IC (104 000 s^{-1}), the amount of BS-IC exhibiting PIDL is higher than that of SD-IC for the following reasons. We discussed the depth dependence of the generation rate of PIDL from the film surface.[26] $^3O_2$ outside the film can penetrate the film surface and diffuse into the interior. Thus, the $[^3O_2]$ on the air side could be larger than that near the substrate, resulting in a large gradient of OQ efficiency from the surface to the substrate. When $[^3O_2]$ is sufficiently high near the air surface, OQ dominates the film even after continuous irradiation, and PIDL is not observed. In the case of BS-IC, OQ was ineffective in suppressing PIDL in most areas of the film because of its small k_Q. Therefore, numerous BS-ICs exhibited PIDL, leading to an enhanced PIDL. In contrast, the k_Q of SD-ICs is high, and OQ becomes dominant over a wide volumetric area, leading to a small number of ICs exhibiting PIDL and a weaker PIDL. This trend is supported by the fact that the PH peak of SD-IC under vacuum *i.e.*, without OQ in the entire area of the film, was higher than the PIDL peak that appeared after continuous irradiation for 15 min (Fig. 5). According to references, a phosphor exhibits a large k_Q in the following cases:[35–38] (I) the integral of the overlap between the emission spectrum of the phosphor and the absorption spectrum of $^3O_2$ is large because OQ occurs *via* a Dexter-type energy transfer mechanism (*i.e.* when the PH wavelength is close to the excitation wavelength of $^3O_2$, 580–1270 nm[39,40]). (II) The quantum yield to generate the T_1 state (= quantum yield of ISC, Φ_{ISC}) is large (>0.4). (III) The lifetime of the T_1 state is long enough to facilitate OQ ($\tau_P > 1$ μs). BS-IC and SD-IC have comparable Φ_{ISC} (0.65 and 0.59) and sufficiently long τ_P (135 and 48 ms) to generate $^1O_2$ by OQ. However, OQ is unlikely to occur in BS-IC because the wavelength of PH (480 nm) is shorter than that of SD-IC (500 nm; Table 1), which is closer to the excitation wavelength of $^3O_2$ (580–1270 nm). Furthermore, the small k_Q of BS-IC is partly attributable to the formation of aggregated structures owing to its planar structure and strong π–π interactions, which was explained by the comparison of calculated and experimental UV-vis spectra (Fig. 2). Accordingly, the probability of collision between $^3O_2$ and BS-IC was relatively

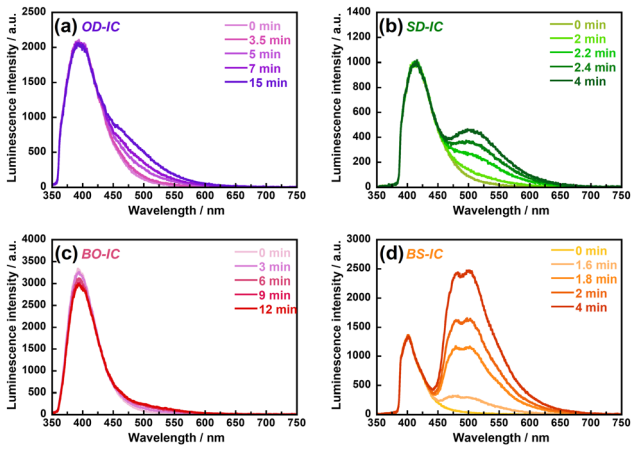

Fig. 6 Irradiation time dependence of the emission spectra of ICs dispersed in PMMA films in air. (a) OD-IC, (b) SD-IC, (c) BO-IC, and (d) BS-IC. The irradiation wavelengths (λ_{ir}) were set to 340 nm for OD-IC and BO-IC and 365 nm for SD-IC and BS-IC.

low, leading to a small k_Q. Here, BO-IC has a planar structure and exhibits strong π–π interactions like BS-IC, which suggests that it may form aggregates and have a small k_Q. However, the k_Q of BO-IC (84 700 s^{-1}) is significantly larger than that of BS-IC (1660 s^{-1}). BS-IC forms aggregates because of its planar structure and inter-sulfur interactions, whereas it is less likely for BO-IC due to the lack of sulfur, which is supported by the fact that aggregate-derived absorption was not observed for BO-IC in Fig. 2. Therefore, BO-IC can collide with $^3O_2$, resulting in a large value of k_Q. Furthermore, the deactivation rate constants of BO-IC from the T_1 to S_0 states (k_P = 0.004 s^{-1}, k_{TS} = 2.76 s^{-1}) were smaller than those of BS-IC (k_P = 0.860 s^{-1}, k_{TS} = 6.55 s^{-1}), resulting in the faster OQ than deactivation. This is another reason for the smaller k_Q.

To investigate the time-dependent increment processes of the PIDL, the emission spectra measured during UV irradiation were decomposed into FL and PIDL spectra, as shown in Fig. S9 (ESI†), and the ratios of the integrated spectral areas were calculated and plotted against irradiation time in Fig. 7. All ICs (OD-IC, SD-IC, BO-IC, and BS-IC) exhibited PIDL after specific induction times (t_{ID} = 3.11, 2.00, 2.05, 1.55 min, respectively). Comparing the structural characters, BO-IC and BS-IC exhibited shorter t_{ID}s than OD-IC and SD-IC, which is attributable to the larger rate constants of ISC (OD-IC: k_{ISC} = 6.02 × 10^{-7} s^{-1}, BO-IC: 24.8 × 10^{-7}, SD-IC: 57.1 × 10^{-7}, BS-IC: 75.5 × 10^{-7}), which generates a large number of triplet excitons and leads to a faster annihilation of $^3O_2$ *via* the OQ process. Similarly, the thioether-bridged SD-IC and BS-IC showed shorter t_{ID}s, which is attributable to the large k_{ISC} owing to the heavy atom effect.[17,19,30] Furthermore, the slopes at the onset of PIDL (S_{on}, the grey dotted line in Fig. 7) for OD-IC and BO-IC with longer t_{ID}s were smaller than those for SD-IC and BS-IC with shorter t_{ID}s. We speculate that there is a depth dependence in t_{ID} due to the depth profile of PIDL efficiency, as described above.[26] Since [$^3O_2$] is larger at the film surface, it takes a longer time to excite all surrounding $^3O_2$ and exhibit PIDL than near the substrate, resulting in a longer t_{ID}. Here, ICs with a high OQ efficiency are more likely to excite $^3O_2$ and exhibit PIDL, and t_{ID} becomes shorter even near the film surface, where [$^3O_2$] is high. Therefore, the t_{ID}s values at the film surface were shorter for SD-IC and BS-IC because of the high OQ efficiencies resulting from the large number of triplet excitons generated by the large k_{ISC}. Consequently, the difference in t_{ID} between the film surface and that near the substrate was smaller for SD-IC and BS-IC, indicating large slopes.

When UV irradiation was stopped after 15 min, the bright green PIDL of the ICs continued for a few seconds. The PIDL lifetime (τ_{PIDL}) estimated from the intensity decay curves of PIDL (Fig. 8) were 0.36, 0.007, 0.57, and 0.41 s for OD-IC, SD-IC, BO-IC, and BS-IC, respectively. The τ_{PIDL} of SD-IC and BS-IC were shorter than those of OD-IC and BO-IC due to the efficient PH decay process owing to the heavy atom effect, leading to the large k_P (Table 2). Furthermore, the τ_{PIDL} of BO-IC and BS-IC were longer than those of OD-IC and SD-IC, originating from the smaller k_{TS}, which is associated with their rigid core structures restricting local molecular motions.

After a sufficient decrease in $^3O_2$ in the films *via* OQ, corresponding to a pseudo-vacuum condition, the PIDL emerged. Therefore, the τ_{PIDL} could become closer to the PH lifetime measured under vacuum. In fact, the τ_{PIDL}s for OD-IC, BO-IC, and BS-IC (τ_{PIDL} = 0.36 s, 0.57 s, 0.41 s) were comparable to the PH lifetimes under vacuum (τ_P = 0.23 s, 0.36 s, 0.14 s). However, the τ_{PIDL} of SD-IC (τ_{PIDL} = 0.007 s) was significantly smaller than the PH lifetime (τ_P = 0.048 s). Because the PIDL decay curves were measured in an open-air system, environmental oxygen was always present inside and outside the film, unlike in a vacuum. Because of the highest OQ rate (k_Q = 104 000 s^{-1}), only a small number of SD-IC exhibited PIDL, as mentioned above; thus, the PIDL was quenched much faster than the other ICs by the $^3O_2$ that diffused after UV irradiation. In contrast, a large number of ICs in OD-, BO-, and BS-ICs, exhibited PIDL due to their small OQ rates (k_Q = 83 800 s^{-1}, 84 700 s^{-1}, 1660 s^{-1}), and thus the PIDL was hardly quenched by $^3O_2$ when UV irradiation

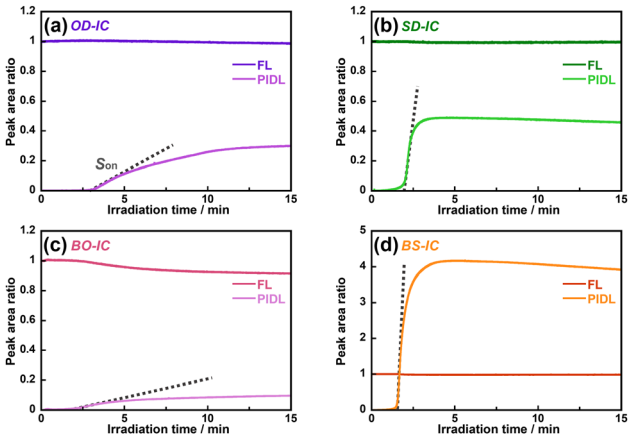

Fig. 7 Time evolution of the emission peak areas during UV irradiation in air for (a) OD-IC, (b) SD-IC, (c) BO-IC, and (d) BS-IC dispersed in PMMA films. The λ_{ir}s of OD-IC and BO-IC was 340 nm and that of SD-IC and BS-IC was 365 nm. The slopes at the onset of PIDL (S_{on}) are shown as a grey dotted line.

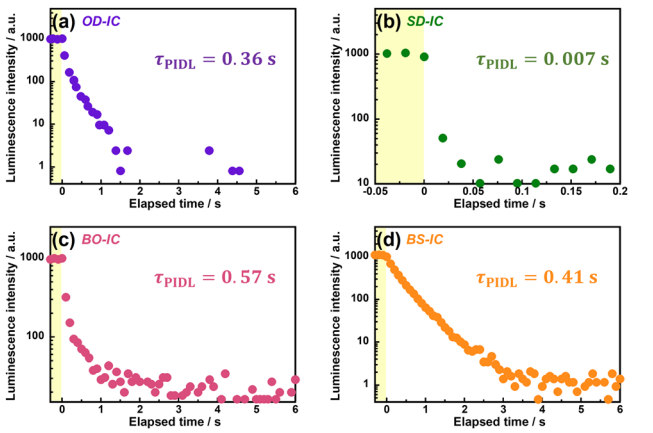

Fig. 8 PIDL decay curves of ICs dispersed in PMMA films for (a) OD-IC (λ_{ir}, λ_{em} = 340, 480 nm), (b) SD-IC (365, 500 nm), (c) BO-IC (340, 470 nm), and (d) BS-IC (365, 480 nm). The irradiation period is presented by yellow hatching.

was stopped. This property could be a reason for the smaller τ_{PIDL} than τ_P for SD-IC. These results indicate that a long τ_{PIDL} can be observed with small values of k_Q and k_{TS}, and BO-IC and BS-IC have suitable rate constants to exhibit longer-lasting PIDL.

4. Conclusions

Four types of ICs, OD-IC, SD-IC, BO-IC, and BS-IC, dispersed in PMMA films showed blue FL at approximately 400 nm in air after UV irradiation for a few seconds, while they exhibited a PH of approximately 500 nm in addition to FL under vacuum. In contrast, when the IC films were continuously irradiated in air for several minutes, they gradually started emitting PIDL from the excited T_1 state. The appearance of the PIDL was caused by a gradual decrease in $^3O_2$ and an increase in $^1O_2$ *via* excitation energy transfer from the ICs in the T_1 state to $^3O_2$, which is called OQ. Owing to the heavy atom effect of the sulfur atom in the core structures, SD-IC and BS-IC exhibited intense PIDL because of the larger number of excitons in the T_1 state, which leads to the shorter induction time (t_{ID}) by the fast decrease in $^3O_2$, and the shorter τ_{PIDL} due to the large k_P than OD-IC and BO-IC. In addition, the π-conjugation in BS-IC extended by the sulfur atom leads to the red shifts of FL and PIDL with decreased band gaps. Comparing the PIDL properties regarding the structural rigidity, owing to the rigid core structures, BO-IC and BS-IC have small k_P due to the suppression of ISC promoted by molecular rotation and conformational change, small k_{TS} relating to molecular motion, and limited local structural relaxation. As a result, these molecules exhibited longer PH lifetimes, shorter induction times, and smaller Stokes shifts than OD-IC and SD-IC, with flexible linkages at their cores. In particular, the newly designed BS-IC showed the most intense PIDL with a short induction time, making it the best IC for observing the PIDL. These results clarified that the following strategies are essential for achieving intense PIDL emission with a short induction time: Introduction of (1) rigid core structure for suppressing k_{TS}, (2) extended π-conjugation exhibiting an intense PH at longer wavelengths, and (3) heavy atoms for promoting k_P and k_{ISC}. Based on the analysis of the optical properties and rate constants of the photophysical processes, this study provides a valuable strategy for the molecular design of PIDL materials and new findings on photophysical processes related to the T_1 state of organic materials.

Author contributions

Marina Doi: resources, data curation, formal analysis, investigation, visualization, methodology, and writing – original draft. Haonan Liu: supervision and visualization. Shinji Ando: conceptualization, supervision, funding acquisition, and project administration.

Data availability

The data supporting this article have been included as part of the ESI.†

Conflicts of interest

There are no conflicts to declare.

Acknowledgements

We wish to thank Ryuichi Isoda and Naiqiang Liang at the Tokyo Institute of Technology for their help with the synthesis of the imide compounds and the discussions. This work was supported by JSPS KAKENHI, Grant Numbers 21H01995 and 22KJ1336.

References

1 J. Zhi, Q. Zhou, H. Shi, Z. An and W. Huang, Organic Room Temperature Phosphorescence Materials for Biomedical Applications, *Chem. – Asian J.*, 2020, **15**, 947–957.
2 H. Shi, W. Yao, W. Ye, H. Ma, W. Huang and Z. An, Ultralong Organic Phosphorescence: From Material Design to Applications, *Acc. Chem. Res.*, 2022, **55**, 3445–3459.
3 X. Wang, H. Ma, M. Gu, C. Lin, N. Gan, Z. Xie, H. Wang, L. Bian, L. Fu, S. Cai, Z. Chi, W. Yao, Z. An, H. Shi and W. Huang, Multicolor Ultralong Organic Phosphorescence through Alkyl Engineering for 4D Coding Applications, *Chem. Mater.*, 2019, **31**, 5584–5591.
4 K. Kanosue and S. Ando, Polyimides with Heavy Halogens Exhibiting Room-Temperature Phosphorescence with Very Large Stokes Shifts, *ACS Macro Lett.*, 2016, **5**, 1301–1305.
5 H. Zhang, J. Jiang, P. Gao, T. Yang, K. Y. Zhang, Z. Chen, S. Liu, W. Huang and Q. Zhao, Dual-Emissive Phosphorescent Polymer Probe for Accurate Temperature Sensing in Living Cells and Zebrafish Using Ratiometric and Phosphorescence Lifetime Imaging Microscopy, *ACS Appl. Mater. Interfaces*, 2018, **10**, 17542–17550.
6 C. A. Derosa, C. Kerr, Z. Fan, M. Kolpaczynska, A. S. Mathew, R. E. Evans, G. Zhang, C. L. Fraser, E. Evans, G. Zhang and C. L. Fraser, Tailoring Oxygen Sensitivity with Halide Substitution in Difluoroboron Dibenzoylmethane Polylactide Materials, *ACS Appl. Mater. Interfaces*, 2015, **7**, 23633–23643.
7 N. J. Turro, V. Ramamurthy and J. C. Scaiano, *Modern Molecular Photochemistry of Organic Molecules*, University Science Books, California, 2010.
8 I. Bhattacharjee and S. Hirata, Highly Efficient Persistent Room-Temperature Phosphorescence from Heavy Atom-Free Molecules Triggered by Hidden Long Phosphorescent Antenna, *Adv. Mater.*, 2020, **32**, 2001348.
9 C. J. Easley, M. Mettry, E. M. Moses, R. J. Hooley and C. J. Bardeen, Boosting the Heavy Atom Effect by Cavitand Encapsulation: Room Temperature Phosphorescence of Pyrene in the Presence of Oxygen, *J. Phys. Chem. A*, 2018, **122**, 6578–6584.
10 P. Irmler and R. F. Winter, Complexes Trans-Pt(BODIPY)X(PEt3)2: Excitation Energy-Dependent Fluorescence and Phosphorescence Emissions, Oxygen Sensing and Photocatalysis, *Dalton Trans.*, 2016, **45**, 10420–10434.

11 H. Sun, R. Ding, S. Lv, S. Zhou, S. Guo, Z. Qian and H. Feng, Clustering-Triggered Ultralong Room-Temperature Phosphorescence of Organic Crystals through Halogen-Mediated Molecular Assembly, *J. Phys. Chem. Lett.*, 2020, **11**, 4962–4969.
12 M. Nara, R. Orita, R. Ishige and S. Ando, White-Light Emission and Tunable Luminescence Colors of Polyimide Copolymers Based on FRET and Room-Temperature Phosphorescence, *ACS Omega*, 2020, **5**, 14831–14841.
13 Z. Yang, C. Xu, W. Li, Z. Mao, X. Ge, Q. Huang, H. Deng, J. Zhao, F. L. Gu, Y. Zhang and Z. Chi, Boosting the Quantum Efficiency of Ultralong Organic Phosphorescence up to 52% via Intramolecular Halogen Bonding, *Angew. Chem., Int. Ed.*, 2020, **59**, 17451–17455.
14 K. Kanosue, S. Hirata, M. Vacha, R. Augulis, V. Gulbinas, R. Ishige and S. Ando, A Colorless Semi-Aromatic Polyimide Derived from a Sterically Hindered Bromine-Substituted Dianhydride Exhibiting Dual Fluorescence and Phosphorescence Emission, *Mater. Chem. Front.*, 2019, **3**, 39–49.
15 M. Doi, K. Muto, M. Nara, N. Liang, K. Sano, H. Mori, R. Ishige and S. Ando, Photoluminescence Properties of Copolyimides Containing Naphthalene Core and Analysis of Excitation Energy Transfer between the Dianhydride Moieties, *J. Photopolym. Sci. Technol.*, 2021, **34**, 423–430.
16 H. Liu, R. Isoda, M. Doi, K. Muto and S. Ando, Pressure-Induced Enhancement of Room-Temperature Phosphorescence in Heavy Halogen-Containing Imide and Polyimide, *J. Phys. Chem. B*, 2024, **128**, 7690–7701.
17 K. Watanabe, I. Osaka, S. Yorozuya and K. Akagi, Helically π-Stacked Thiophene-Based Copolymers with Circularly Polarized Fluorescence: High Dissymmetry Factors Enhanced by Self-Ordering in Chiral Nematic Liquid Crystal Phase, *Chem. Mater.*, 2012, **24**, 1011–1024.
18 B. H. Drummond, G. C. Hoover, A. J. Gillett, N. Aizawa, W. K. Myers, B. T. Mcallister, S. T. E. Jones, Y.-J. Pu, D. Credgington and D. S. Seferos, Selenium substitution enhances reverse intersystem crossing in a delayed fluorescence emitter, *J. Phys. Chem. C*, 2020, **124**, 6364.
19 J. Sivanarayanan, E. Sebastian, K. Vinod and M. Hariharan, Ultrafast Intersystem Crossing in Selenium-Annulated Perylene Bisimide, *J. Phys. Chem. C*, 2022, **126**, 13319–13326.
20 H. Marchi Luciano, G. Farias, C. M. Salla, L. G. Franca, S. Kuila, A. P. Monkman, F. Durola, I. H. Bechtold, H. Bock and H. Gallardo, Room Temperature Phosphorescence in Solution from Thiophene-Bridged Triply Donor-Substituted Tristriazolotriazines, *Chem. – Eur. J.*, 2023, **29**, e202203800.
21 F. Xiao, H. Gao, Y. Lei, W. Dai, M. Liu, X. Zheng, Z. Cai, X. Huang, H. Wu and D. Ding, Guest-host doped strategy for constructing ultralong-lifetime near-infrared organic phosphorescence materials for bioimaging, *Nat. Commun.*, 2022, **13**, 186.
22 L. Gu, H. Wu, H. Ma, W. Ye, W. Jia, H. Wang, H. Chen, N. Zhang, D. Wang, C. Qian, Z. An, W. Huang and Y. Zhao, Color-Tunable Ultralong Organic Room Temperature Phosphorescence from a Multicomponent Copolymer, *Nat. Commun.*, 2020, **11**, 1–8.
23 M. Nara, E. Fujiwara, A. Vyšniauskas, V. Gulbinas and S. Ando, Photophysical analysis of dual fluorescence and phosphorescence emissions observed for semi-aliphatic polyimides at lower temperatures, *Phys. Chem. Chem. Phys.*, 2024, **26**(21), 15461–15471.
24 M. Louis, H. Thomas, M. Gmelch, A. Haft, F. Fries and S. Reineke, Blue-Light-Absorbing Thin Films Showing Ultralong Room-Temperature Phosphorescence, *Adv. Mater.*, 2019, **31**, 1807887.
25 Y. Zhang, L. Gao, X. Zheng, Z. Wang, C. Yang, H. Tang, L. Qu, Y. Li and Y. Zhao, Ultraviolet irradiation-responsive dynamic ultralong organic phosphorescence in polymeric systems, *Nat. Commun.*, 2021, **12**, 1–9.
26 M. Doi, R. Ishige and S. Ando, Long-Lived Luminescence Emitted from Imide Compounds Dispersed in Polymer Matrices after Continuous Ultraviolet Irradiation and its Relation to Oxygen Quenching, *ChemPhotoChem*, 2023, **7**, e202200310.
27 S. Ando, T. Matsuura and S. Sasaki, Coloration of Aromatic Polyimides and Electronic Properties of Their Source Materials, *Polym. J.*, 1997, **29**, 69–76.
28 J. Wakita, H. Sekino, K. Sakai, Y. Urano and S. Ando, Molecular Design, Synthesis, and Properties of Highly Fluorescent Polyimides, *J. Phys. Chem. B*, 2009, **113**, 15212–15224.
29 C. Mitsui, M. Yamagishi, R. Shikata, H. Ishii, T. Matsushita, K. Nakahara, M. Yano, H. Sato, A. Yamano, J. Takeya and T. Okamoto, Oxygen- and Sulfur-Bridged Bianthracene V-Shaped Organic Semiconductors, *Bull. Chem. Soc. Jpn.*, 2017, **90**, 931–938.
30 Y. Wen, H. Liu, S. T. Zhang, G. Pan, Z. Yang, T. Lu, B. Li, J. Cao and B. Yang, Modulating Room Temperature Phosphorescence by Oxidation of Thianthrene to Achieve Pure Organic Single-Molecule White-Light Emission, *CCS Chem.*, 2021, **3**, 1940–1948.
31 H. Liu, Y. Gao, J. Cao, T. Li, Y. Wen, Y. Ge, L. Zhang, G. Pan, T. Zhou and B. Yang, Efficient Room-Temperature Phosphorescence Based on a Pure Organic Sulfur-Containing Heterocycle: Folding-Induced Spin–Orbit Coupling Enhancement, *Mater. Chem. Front.*, 2018, **2**, 1853–1858.
32 C. Yuan, S. Saito, C. Camacho, S. Irle, I. Hisaki and S. Yamaguchi, A π-conjugated system with flexibility and rigidity that shows environment-dependent RGB luminescence, *J. Am. Chem. Soc.*, 2013, **135**, 8842–8845.
33 Z. Yang, Z. Fu, H. Liu, M. Wu, N. Li, K. Wang, S.-T. Zhang, B. Zou and B. Yang, Pressure-induced room-temperature phosphorescence enhancement based on purely organic molecules with a folded geometry, *Chem. Sci.*, 2023, **14**, 2640–2645.
34 Y. Shoji, Y. Ikabata, Q. Wang, D. Nemoto, A. Sakamoto, N. Tanaka, J. Seino, H. Nakai and T. Fukushima, Unveiling a New Aspect of Simple Arylboronic Esters: Long-Lived Room-Temperature Phosphorescence from Heavy-Atom-Free Molecules, *J. Am. Chem. Soc.*, 2017, **139**, 2728.
35 E. L. Clennan, New Mechanistic and Synthetic Aspects of Singlet Oxygen Chemistry, *Tetrahedron*, 2000, **56**, 9151.
36 H.-G. Jeong and M.-S. Choi, Design and Properties of Porphyrin-based Singlet Oxygen Generator, *Isr. J. Chem.*, 2016, **56**, 110.

37 M. C. Derosa and R. J. Crutchley, Photosensitized singlet oxygen and its applications, *Coord. Chem. Rev.*, 2002, **233**, 351.
38 N. Mehraban and H. S. Freeman, Developments in PDT Sensitizers for Increased Selectivity and Singlet Oxygen Production, *Materials*, 2015, **8**, 4421–4456.
39 A. Blázquez-Castro, Direct 1O2 Optical Excitation: A Tool for Redox Biology, *Redox Biol.*, 2017, **13**, 39–59.
40 A. A. Krasnovsky, Luminescence and Photochemical Studies of Singlet Oxygen Photonics, *J. Photochem. Photobiol., A*, 2008, **196**, 210–218.

